Ultrafast Primary Processes in PS I from *Synechocystis* sp. PCC 6803: Roles of P700 and A_0

Sergei Savikhin,* Wu Xu,† Parag R. Chitnis,*† and Walter S. Struve*‡
*Ames Laboratory, U. S. Department of Energy, and Departments of †Biochemistry, Biophysics, and Molecular Biology, and ‡Chemistry, Iowa State University, Ames, Iowa 50011 USA

ABSTRACT The excitation transport and trapping kinetics of core antenna-reaction center complexes from photosystem I of wild-type *Synechocystis* sp. PCC 6803 were investigated under annihilation-free conditions in complexes with open and closed reaction centers. For closed reaction centers, the long-component decay-associated spectrum (DAS) from global analysis of absorption difference spectra excited at 660 nm is essentially flat (maximum amplitude $<10^{-5}$ absorbance units). For open reaction centers, the long-time spectrum (which exhibits photobleaching maxima at ~680 and 700 nm, and an absorbance feature near 690 nm) resembles one previously attributed to ($P700^+$ - P700). For photosystem I complexes excited at 660 nm with open reaction centers, the equilibration between the bulk antenna and far-red chlorophylls absorbing at wavelengths >700 nm is well described by a single DAS component with lifetime 2.3 ps. For closed reaction centers, two DAS components (2.0 and 6.5 ps) are required to fit the kinetics. The overall trapping time at P700 (~24 ps) is very nearly the same in either case. Our results support a scenario in which the time constant for the P700 → A_0 electron transfer is 9–10 ps, whereas the kinetics of the subsequent $A_0 \rightarrow A_1$ electron transfer are still unknown.

INTRODUCTION

The primary events triggered by light absorption in the chlorophyll (Chl) *a* core antenna of photosystem I (PS I) complexes have been intensively studied by many groups since the mid-1980s (for a review, see van Grondelle et al., 1994). In recent years, a consensus has begun to emerge regarding some of the principal features of the experimental PS I antenna kinetics (Holzwarth et al., 1990, 1993; Jia et al., 1992; Holzwarth, 1991, 1992; Turconi et al., 1993; Hecks et al., 1994; Hastings et al., 1995; Savikhin et al., 1999). The Chl *a* Q_y antenna spectrum in PS I is broad, owing to the presence of multiple Chl spectral forms absorbing between ~660 and 700 nm (Ikegami and Itoh, 1986; Owens et al., 1988; Jia et al., 1992; van der Lee et al., 1993; Gobets et al., 1994). When this spectrum is excited toward its blue edge, subpicosecond equilibration occurs among the ~100 Chl pigments in the bulk antenna (Du et al., 1993; Hastings et al., 1994a,b, 1995; Savikhin et al., 1999). Subsequent equilibration then occurs (with 3–7 ps kinetics, depending on species) with a small number of specialized red Chls absorbing at wavelengths >700 nm. The number and type of these far-red Chls varies with the species. The bulk antenna excitation in cyanobacterial and green plant PS I complexes with open reaction centers decays with 19–24 ps kinetics, due to trapping at P700 (Hastings et al., 1995). (P700 designates the primary donor special pair Chls; P700*, electronically excited P700; and $P700^+$, oxidized P700.) Very similar trapping kinetics (arising from an unknown mechanism) reportedly occur in complexes with closed reaction centers, in which the special pair has been oxidized to $P700^+$. The cause for the apparent similarity between the trapping kinetics in complexes with open and closed reaction centers is unknown and appears to have been little discussed in the literature.

Several major issues persist regarding the primary photoprocesses in PS I. Although the structure of a cyanobacterial PS I core antenna-reaction center complex has become increasingly well known since 1993 (Krauss et al., 1993, 1996), the locations and functions of the far-red Chls, whose Q_y levels lie at wavelengths longer than the P700 lower exciton component, are still unknown. Several authors have proposed that the red Chls are close to the reaction center (Werst et al., 1992; Jia et al., 1992; Trinkunas and Holzwarth, 1994). The fluorescence excitation spectrum of PS I trimers from the cyanobacterium *Spirulina platensis* exhibits a 738 nm band at 77 K, in addition to shorter-wavelength features at 680 and 710 nm (Karapetyan et al., 1997). The 738 nm band is absent in the monomeric complexes, suggesting that the longest-wavelength Chl type in *Spirulina* arises from interactions among peripheral Chls bound to different monomers within the trimer. Different fluorescence behavior is shown by PS I trimers from the cyanobacterium *Synechocystis* sp. PCC 6803, whose low-temperature spectrum is dominated by an intense band at ~718 nm (Gobets et al., 1994). These authors concluded that essentially all of the far-red absorption and emission in *Synechocystis* arises from a single dimeric Chl pair absorbing at 708 nm. They reasoned that the unusually large (~200 cm^{-1}) Stokes' shift of the 718 nm emission band with respect to the 708 nm absorption peak stems from a large reorganization energy, analogous to that which accompanies charge-transfer transitions in the B820 $BChl_2$ dimer (Pullerits et al., 1994) and in the special pair BChls of bacterial reaction centers (Reddy et al., 1992). Soukoulis et

Received for publication 24 February 2000 and in final form 22 May 2000.
Address reprint requests to Dr. Walter S. Struve, Iowa State University, Department of Chemistry, Gilman Hall, Ames, IA 50011-3111. Tel.: 515-294-4276; Fax: 515-294-1699; E-mail: wstruve@ameslab.gov.

0006-3495/00/09/1573/14 $2.00

al. (1999) sought to localize the position of the F718 Chl(s) in *Synechocystis* sp. by studying the fluorescence spectra in monomeric and trimeric PS I mutants deficient in one or more of the peripheral protein subunits PsaF/J, PsaK, PsaI/L, and PsaM (Fig. 1). All of the subunit-deficient mutants (monomeric as well as trimeric) exhibited fluorescence spectra essentially identical to the wild-type spectrum. The F718 Chl(s) in *Synechocystis* is (are) therefore likely bound to the PsaA/B heterodimer, which binds the reaction center cofactors as well as the majority of bulk antenna Chls. Since PsaA/B binds the most distant as well as nearest antenna Chls (>50 Å and <30 Å, respectively, from the reaction center), the location of the F718 Chls with respect to the reaction center is still unresolved. (The notations F*xxx* and C*xxx* represent, respectively, Chl species with low-temperature Q_y fluorescence peak at *xxx* nm and those with low-temperature Q_y absorption peak at *xxx* nm.) Very recent spectral hole-burning studies of wild-type and mutant PS I from *Synechocystis* (Rätsep et al., 2000) have detected separate low-temperature absorption bands at 708 and 714 nm, so that the C708 and F718 features in fact arise from different states. The 718 nm fluorescence in *Synechocystis* is thus due to the C714 Chls, rather than the C708 Chls as reported earlier (Gobets et al., 1994).

The kinetic sequence of electron transfer events in PS I after oxidation of P700 is not well established. A review by Brettel (1997) suggests that electron transfer from P700* to the chlorophylloid primary acceptor (A_0) occurs with 1- 3 ps kinetics, followed by 20–50 ps electron transfer from A_0 to the phylloquinone secondary acceptor, A_1. Because the antenna and reaction center Chl absorption spectra overlap considerably, and because selective excitation of reaction center cofactors like P700 or A_0 is not possible, these electron transfer timescales are necessarily based on indirect or cumulative measurements. Hastings et al. (1994b) determined that the difference between the 590 → 686 nm absorption difference profiles for *Synechocystis* PS I particles with open and closed reaction centers (prepared under neutral and oxidizing conditions) exhibited ~4 ps photobleaching/stimulated emission (PB/SE) rise and ~21 ps PB/SE decay kinetics. (The notation *xxx* → *yyy* denotes a pump-probe experiment in which an absorption difference profile was measured at *yyy* nm after excitation at *xxx* nm.) These lifetimes were attributed to the formation and disappearance, respectively, of the radical pair ($P700^+$ A_0^-) following unselective Q_x excitation of the bulk antenna at 590 nm. Thus, the 21 ps kinetics were ascribed to the electron transfer step $A_0 \rightarrow A_1$. The ~4 ps kinetics were assigned to the sequence beginning with light absorption absorption in the antenna, continuing with antenna excitation equilibration and trapping at P700, and ending with reduction of A_0. Under this interpretation, the rate-limiting step in this sequence (which would normally require ~20 ps in *Synechocystis* sp. under annihilation-free conditions) was foreshortened to ~4 ps under the high-intensity laser pumping required in order to observe absorption difference signals with useful signal/noise ratio (Hastings et al., 1994b). Hence, these measurements represented an upper bound of ~4 ps for the timescale of the process P700 $A_0 \rightarrow P700^+$ A_0^-. This conclusion rested on the key assumption, stressed by Hastings et al. (1994b), that the antenna kinetics are identical in PS I complexes with open and closed reaction centers, and therefore cancel out in the (open-closed) absorption difference spectra. In an earlier paper (Hastings et al., 1994a), the intrinsic rate of radical pair formation was estimated to be ~1.6 ps in a trapping-limited kinetic model using an assumed effective antenna size. The latter was derived from crude estimates of the core antenna size (~100), the antenna spectral distribution, and the number of far-red Chls (believed to be ~8) absorbing at ~703 nm at room temperature. Hastings et al. (1994b) reasonably concluded that the difficulty of measuring an (A_0 - A_0^-) transient spectrum (which was believed to peak at ~686 nm) stems from lack of A_0^- population buildup, due to its relatively short lifetime.

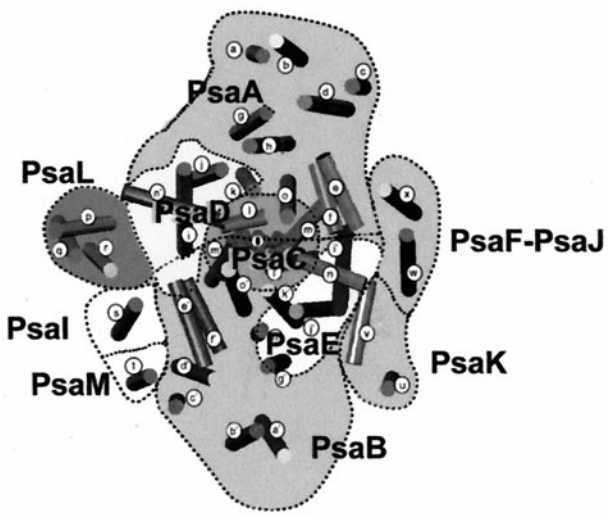

FIGURE 1 Arrangement of protein subunits in the core antenna - reaction center complex of cyanobacterial photosystem I, according to 4 Å structure of Krauss et al. (1995), with subsequent modifications. The reaction center cofactors lie at the boundary between the PsaA and PsaB subunits, directly below subunit PsaC.

The positions of Chls inside PS I reaction centers from the cyanobacterium *Synechococcus elongatus* (Krauss et al., 1996) resemble the pigment organization in purple bacterial reaction centers (Chang et al., 1991; Deisenhofer et al., 1985; Deisenhofer and Michel, 1989; Allen et al., 1986). The primary electron acceptor A_0 is believed to occupy (one of) the position(s) similar to the locations of the bacterial BPheos; the (A_0 - A_0^-) absorption difference spectrum reportedly exhibits a maximum at ~686 nm (Hastings et al., 1994b). However, no absorption transient attributable to the PS I analogs of the accessory BChls (hereafter termed the "accessory Chls") has been reported.

In this paper, we report new pump-probe experiments on wild-type PS I trimers from *Synechocystis* sp. PCC 6803. All of our experiments were performed under annihilation-free conditions, as verified by in situ power dependence measurements. Building on the foundations laid by Hastings et al. (1994b), we evaluated differences between pump-probe profiles for open and closed reaction centers, obtained for the same sample under identical spectroscopic conditions. Direct subtraction was thus possible without renormalization. Since the presence of a C714 far-red Chl species was indicated by spectral hole-burning experiments in *Synechocystis* sp. (Rätsep et al., 2000), many of our PS I samples were excited at 718 nm as well as at 660 nm. We believe that the bulk of the absorption at 718 nm occurs in the C714 species (see below), although a small fraction (~10%) of light at this wavelength is absorbed in the P700 lower exciton level.

MATERIALS AND METHODS

Trimeric PS I complexes were purified from the wild-type strain of the cyanobacterium *Synechocystis* sp. PCC 6803 by a previously published method (Sun et al., 1998). Optical clarity of the PSI preparation was improved by centrifugation through Spin-X centrifuge filter units (0.22 μm cellulose acetate membrane; Costar). The chlorophyll concentration of PS I trimers was measured in 80% acetone. Purity of PS I preparations was examined by sodium dodecyl sulfate-polyacrylamide gel electrophoresis analysis of protein subunits.

A self-mode-locked Ti:sapphire laser (pumped by a 3W multiline Coherent Radiation Innova 90–5 argon ion laser, Santa Clara, CA) generated 780 nm pulses with 50–80 fs duration at 100 MHz repetition rate. These were passed through an optical isolator, and dispersed to ~150 ps duration in a grating pulse stretcher. The pulses were then amplified by a factor of $\sim 10^6$ at 1 kHz (0.5 mJ/pulse) in a Ti:sapphire regenerative amplifier, pumped by a Clark-MXR Inc, ORC-1000 Q-switched Nd:YAG laser (Dexter, MI). The regenerative amplifier incorporated a Medox Electro-Optics Pockels cell. After recompression to 90–100 fs duration in a dual grating pulse compressor, the amplified pulses were converted in a Type I BBO optical parametric amplifier (OPA) crystal into infrared signal and idler frequencies ($\omega \rightarrow \omega_1 + \omega_2$). The OPA design, after that of Hasson (1997), employed a double-pass configuration; the OPA process was initiated by continuum seed pulses generated by focusing <1% of the 780 nm pulses into a sapphire crystal. This seeding greatly increased the signal/noise in the OPA signal pulses. Frequency-doubling the OPA signal output pulses yielded visible light pulses that were easily tunable over the entire photosystem I Chl *a* Q_y spectrum (600–720 nm). Aside from the argon ion and Nd:YAG pump lasers, all major optical assemblies (including the regenerative amplifier) were built in-house. A Gaussian fit to a Kerr-effect cross-correlation profile between 680 nm frequency-doubled signal pulses and 700 nm broadband continuum pulses generated in a sapphire plate yielded 98 fs full width at half maximum (fwhm), which would correspond to 70 fs fwhm laser pulses if the signal and continuum pulse profiles had identical shapes. Cross-correlations at other wavelengths varied from 100 to 200 fs fwhm. Due to group velocity dispersion in the optics, the timing between pump and probe pulses varied with wavelength (by ~400 fs for probe wavelengths between 650 and 730 nm); this was calibrated for all combinations of pump and probe wavelengths.

For pump-probe experiments, frequency-doubled OPA signal pulses served as pump pulses, while the broadband continuum pulses sampled the PS I ΔA spectrum at variable time delays. Continuum pulses were split into reference and probe beams; both were focussed into the PS I sample cell, but only the probe beam intersected the pump beam. The reference and probe beams were dispersed in a programmable Oriel MS257 imaging monochromator with 1200 groove/mm grating operated at ~3 nm bandpass, and directed onto separate Hamamatsu S3071 Si pin photodiodes (5 mm diameter active area). The photodiode signals for every pulse were amplified and integrated in Stanford Research Systems SR250 boxcar integrators, and digitized in a National Instruments MIO-000 16-bit analog-to-digital converter (ADC) computer plug-in module. The time delay sweep and monochromator drive were automated with Spectra-Solve software (Ames Photonics, Inc., Ames, IA), and a ΔA surface versus time and probe wavelength (e.g., 15 probe wavelengths from 660 to 700 nm) could be generated in ~2 h without realignment of lasers or optics. The noise performance was close to shot noise-limited; the rms noise in dA was $\sim 10^{-5}$ for 1 s accumulation time. Photosystem I samples were housed in ~0.7 mm path length, 2-inch diameter centrifugal cells rotating at ~10 Hz; given the 1 kHz laser repetition rate, successive pulses excited nonoverlapping spots in the cell. The PS I optical density was typically ~0.4 at 680 nm. Excitation pulse energies were <10 nJ, and the excited spot size was ~100 μm. In all current experiments, operation in the annihilation-free regime was confirmed by control studies in which the laser power was varied. Fig. 3 in Savikhin et al. (1999), which illustrates the strong pump power dependence of 660 → 700 nm pump-probe profiles for PS I from *Synechocystis* sp. in the annihilation regime, shows an example of such a control study. Unless otherwise specified, experiments were carried out with linear pump and probe polarizations separated by 54.7°. All experiments were performed at room temperature. In anisotropy studies, the pump and probe polarizations were rapidly alternated between parallel and perpendicular using a Meadowlark Optics LRC-200-IR1 liquid crystal variable retarder (Longmont, CO); the optical anisotropy was then computed from the respective absorption difference signals $\Delta A_{\parallel}(t)$, $\Delta A_{\perp}(t)$ via

$$r(t) = (\Delta A_{\parallel}(t) - \Delta A_{\perp}(t)/(\Delta A_{\parallel}(t) + 2\Delta A_{\perp}(t)).$$

All PS I samples for pump-probe experiments contained 5 mM sodium ascorbate. The P700 oxidation state was reversibly controlled by ambient lighting conditions; no differential chemical treatments were required to prepare open or closed reaction centers. Reaction centers in pump-probe experiments conducted in complete darkness were predominantly open (cf. Results section below). In experiments performed on samples continuously illuminated by a computer-controlled 3V flashlight bulb, the reaction centers were almost exclusively closed. Our ability to manipulate the P700 oxidation state reversibly without sample replacement or system realignment ensured exact mutual normalization of absorption difference signals for open and closed reaction centers.

The steady-state absorption spectrum for PS I with open reaction centers was obtained with a sample in a dark compartment of a Perkin-Elmer Lambda 3 spectrophotometer (Norwalk, CT). Continuous stirring of the solution with an 8 mm magnetic bar minimized $P700^+$ buildup in the light beam path. For closed reaction centers, the same sample was illuminated in situ for 2 s with a computer-controlled 3V flashlight bulb. After the light was turned off for 3 s, the sample absorbance was measured. This automated sequence was repeated for the entire set of absorbance wavelengths required in a spectrum. This protocol was necessitated because absorbance measurements during lightbulb illumination were precluded by scattered light in the spectrophotometer. The 3 s delay (several times longer than the 0.5 s spectrophotometer time constant, but ~2 orders of magnitude shorter than the 100–200 s $P700^+ \rightarrow$ P700 recombination time determined in separate experiments, not shown) yielded accurate measurement of the spectrum for closed reaction centers. The difference between the absorption spectra for open and closed reaction centers is shown in Fig. 2, along with the steady-state absorption spectrum for PS I with open reaction centers.

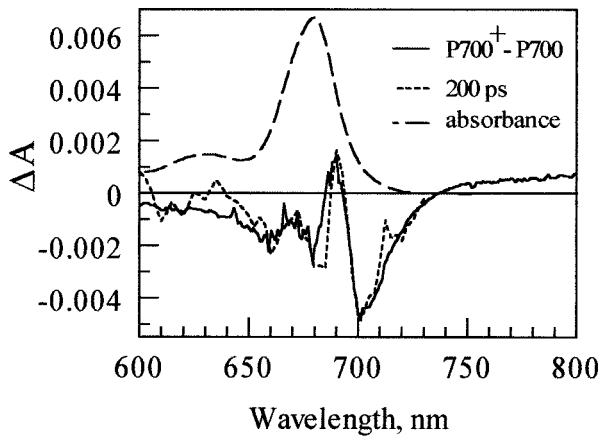

FIGURE 2 Difference between steady-state absorption spectra for PS I complexes with closed and open reaction centers (*solid curve*); steady-state absorption spectrum of PS I with open reaction centers (*dashed curve*); and absorption difference spectrum at 200 ps for PS I with open reaction centers (*dotted curve*). The 200 ps ΔA spectrum and the steady state spectrum for open reaction centers are multiplied by factors of 12 and 0.01, respectively.

RESULTS

Global analyses for open and closed reaction centers

Pump-probe experiments under 660 nm excitation in complete darkness yielded the decay-associated spectra (DAS) shown in Fig. 3, *a* and *b*. With the room lights on and/or a flashlight directed into the sample, the otherwise identical pump-probe experiment yielded the DAS shown in Fig. 3 *c*. Family resemblances shared by the three sets of DAS include: (i) a 400–530 fs DAS component arising from subpicosecond excitation equilibration in the bulk antenna; (ii) a ~2 ps component signaling equilibration between the bulk antenna and far-red Chl(s) absorbing at 705–710 nm; and (iii) a 22–24 ps component due to excitation trapping at the reaction center. A major difference between the analyses of the light and dark experiments lies in the asymptotic spectrum at long times. The long-time DAS labeled "1.2 ns" in Fig. 3, *a* and *b*, for dark reaction centers exhibits PB/SE maxima at ~680 and 700 nm, coupled with an absorption maximum at ~690 nm. This spectrum is essentially the same as one previously identified as the ($P700^+A_0^-$) - (P700 A_0) difference spectrum for *Synechocystis* sp. (Hastings et al., 1994a,b). By constrast, the long-time spectrum labeled "10.8 ns" in Fig. 3 *c* for reaction centers in ambient light appears flat. The long-component DAS for dark reaction centers (Fig. 3, *a* and *b*) is very similar to the difference between steady-state absorption spectra for PS I with closed and open reaction centers (Fig. 2). The absorption difference spectrum measured for open reaction centers at 200 ps time delay is superimposable on the steady-state absorption difference spectrum (Fig. 2). Hence, the PS I complexes in Fig. 3, *a* and *b*, and Fig. 3 *c* contain primarily open and closed reaction centers, respectively.

Another difference between the DAS for open and closed reaction centers was that a fifth DAS component (lifetime 6.5 ps) was required for accurate description of the kinetics for closed reaction centers at most probe wavelengths (Fig. 3 *c*). Such an additional component was not usually required for open reaction centers (Fig. 3, *a* and *b*). At probe wavelengths other than 695 nm, a four-component global analysis (yielding lifetimes of 530 fs, 2.3 ps, 23.6 ps, and 1.2 ns) provides a good description of the kinetics for open reaction centers. The additional, minor 6.2 ps component that emerges in a five-component global analysis for open reaction centers (Fig. 3 *b*) shows a relatively low, fluctuating amplitude at most wavelengths.

Our previously measured PS I kinetics (Savikhin et al., 1999), obtained under the assumption that the P700 oxidation state does not influence antenna processes, coincide with our present results for closed reaction centers. Structure-based simulations of PS I antenna kinetics (Savikhin and Struve, unpublished work) in fact predict that the overall antenna equilibration kinetics depend to some extent on whether the reaction centers are open or closed. Thus, contrasting antenna kinetics as well as reaction center processes may contribute to the total differences observed between the kinetics for open and closed reaction centers.

Individual profiles excited at 660 nm and 718 nm

Fig. 4 shows 660 → 690 nm isotropic absorption difference profiles for PS I complexes with open and closed reaction centers. The corresponding (open-closed) difference profile is shown in the bottom of Fig. 4. For open and closed reaction centers, the ΔA signals at long times are >0 and ~ 0, respectively. These are consistent with the relative long-component DAS amplitudes shown for open and closed reaction centers at 690 nm in Fig. 3. The 660 → 690 nm difference profile (bottom of Fig. 4) initializes to ~0 at zero time. (The mutual normalization of the open and closed profiles is exact, because the two experiments were conducted for the same PS I sample with identical cell position and laser beam geometries.) A biexponential fit to this difference signal yields a 9.8 ps PB/SE rise time, combined with a 21 ps PB/SE decay toward a positive asymptote. This positive asymptotic feature corresponds to the 690 nm absorption peak in the steady-state (open-closed) spectrum (Fig. 2). (This difference signal could, alternatively, be interpreted as a 9.8 absorption decay feature, followed by 21 ps absorption rise kinetics. Our experiments also cannot discern a priori whether the difference kinetics are due to processes occurring in open reaction centers alone, processes in closed reaction centers alone, or to different extents in both.) This difference profile resembles one described by Hastings et al. (1994b) for *Synechocystis* sp.,

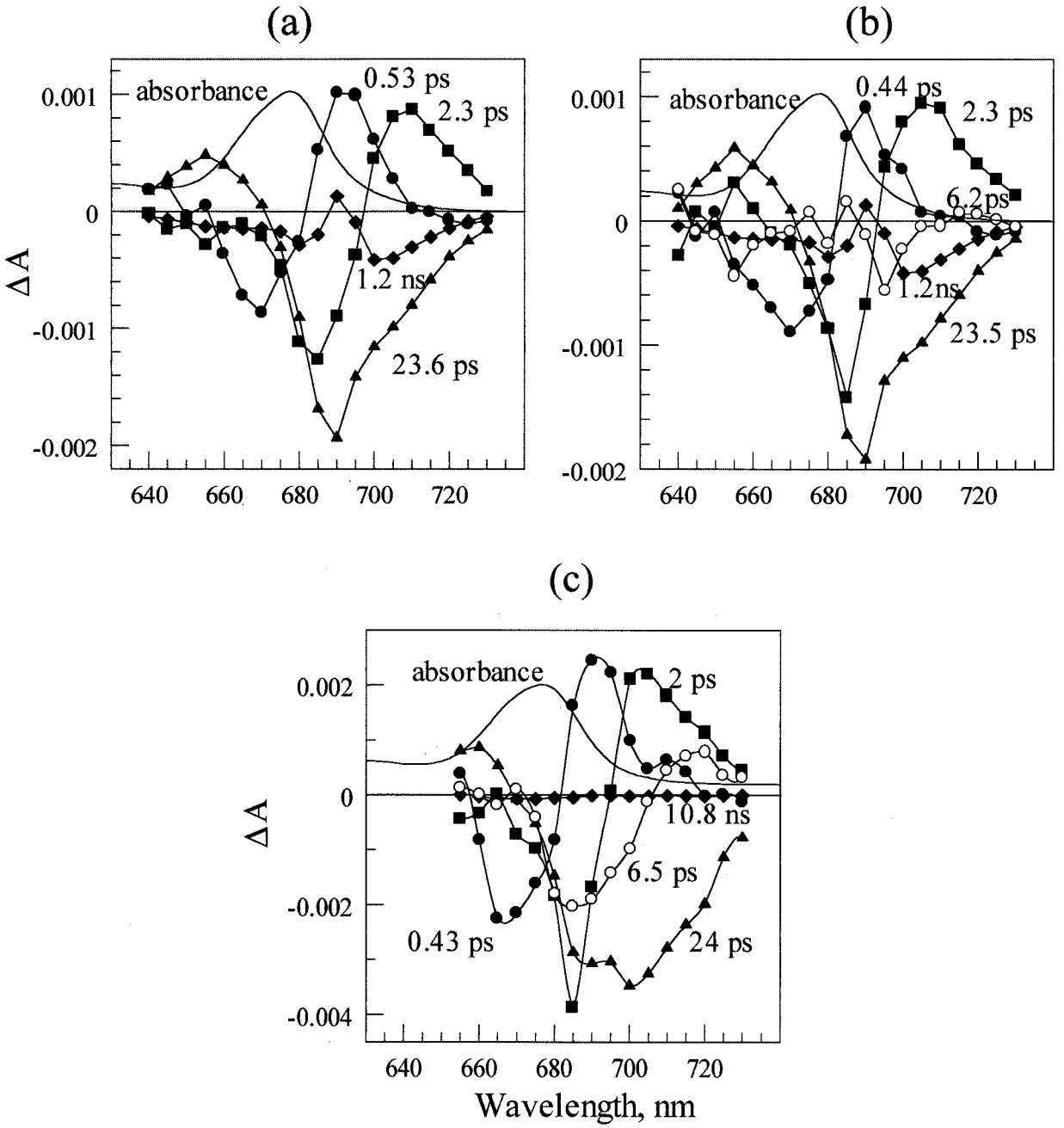

FIGURE 3 Decay-associated spectra (DAS) from global analyses of pump-probe experiments on photosystem I from *Synechocystis* sp. excited at 660 nm: (*a*) four-component fit for open reaction centers; (*b*) five-component fit for open reaction centers; and (*c*) five-component fit for closed reaction centers. Negative amplitudes correspond to PB/SE decay and/or excited state absorption rise components. Absorbance units are absolute under present experimental conditions. Steady-state absorption spectrum (*solid curve*) is superimposed on each set of DAS. DAS spectral components in (*a*) are 0.53 ps (●), 2.3 ps (■), 23.6 ps (▲), and 1.2 ns (♦); in (*b*), 0.44 ps (●), 2.3 ps (■), 6.2 ps (○), 23.5 ps (▲), and 1.2 ns (♦); and in (*c*), 0.43 ps (●), 2.0 ps (■), 6.5 ps (○), 24 ps (▲), and 10800 ps (♦).

excited at 590 nm and probed at 686 nm. These authors extracted biexponential lifetimes of 4 and 21 ps for their difference profile, analogous to our 9.8 and 21 ps kinetics. These kinetics were attributed largely to formation and decay of the (A_0^- - A_0) difference spectrum, *via* the electron transfer sequence P700* A_0 $A_1 \rightarrow P700^+$ A_0^- $A_1 \rightarrow P700^+$ A_0 A_1^-. The rate-limiting step for A_0^- formation after antenna excitation is believed to be antenna excitation trapping at P700, which normally requires ~20 ps. Hastings et al. (1994b) ascribed the apparent 4 ps A_0 reduction kinetics to shortening of the empirical trapping time to ~4 ps due to annihilation in the antenna.

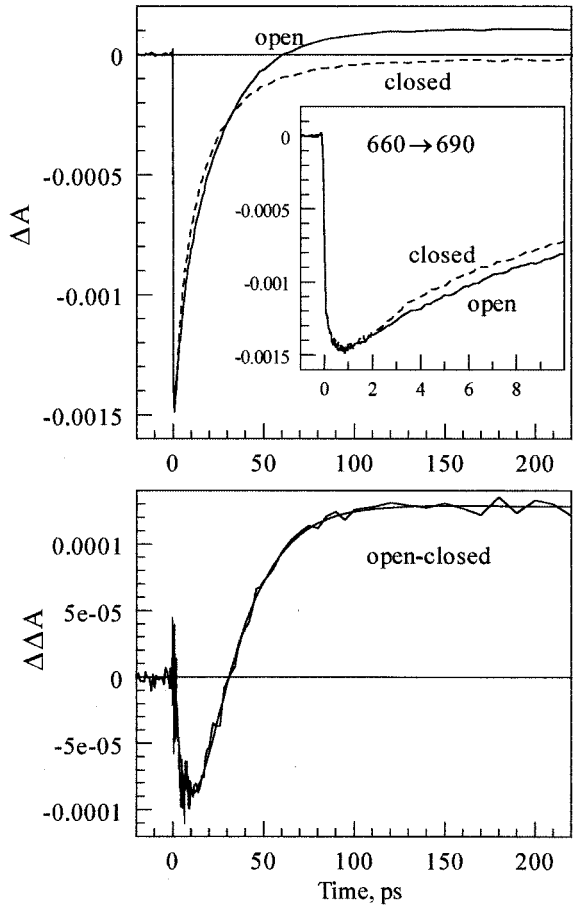

FIGURE 4 Isotropic absorption difference profiles for PS I excited at 660 nm and probed at 690 nm (*Top*) $\Delta A(t)$ for open reaction centers (*solid line*) and $\Delta A(t)$ for closed reaction centers (*dashed line*). (*Bottom*) Difference between isotropic profiles for open and closed reaction centers. Negative signals correspond to PB/SE; signals for open and closed reaction centers are mutually normalized. Absorption changes on vertical scales are in absolute units here and elsewhere.

However, our difference profile in the bottom of Fig. 4 was obtained under annihilation-free conditions (cf. the 23–24 ps trapping components observed for both open and closed reaction centers, Fig. 3). This rules out the interpretation of Hastings et al. (1994b), and our difference signal must therefore arise from some other mechanism (see Discussion).

Fig. 5 shows analogous results for the pump-probe wavelengths 660 → 680, 660 → 700, and 660 → 720 nm. For open reaction centers, the asymptotic signals at long times conform to the relative long-component DAS amplitudes for open reaction centers at the relevant probe wavelengths (Fig. 3). For example, the long-time signal in the 660 → 700 nm experiment is dominated by a PB/SE component, which is consistent with the presence of the 700 PB/SE peak in the long component DAS in the global analysis (Fig. 3). Fitting parameters are listed for multiexponential analyses of the individual and (open-closed) difference profiles in Table 1. All of the difference profiles obtained under 660 nm excitation initialize near 0 at zero time (Figs. 4, 5). The unusual behavior observed at early times (<15 ps) in the 660 → 720 nm difference signal cannot be modeled using a single PB/SE risetime, but can be simulated with rise and decay components of slightly different lifetime but opposite sign. This points to the likelihood that the kinetics for open and closed reaction centers do not share the same set of lifetimes, which complicates the interpretation considerably.

Fig. 6 shows individual isotropic profiles and (open-closed) difference profiles for PS I excited at 718 nm and probed at 680, 690, 710, and 720 nm.

Anisotropy under far-red excitation

In a previous paper (Savikhin et al., 1999), it was shown that excitation in the bulk antenna (pump wavelengths <700 nm) produces pump-probe anisotropies $r(t)$ that decay rapidly (with significant subpicosecond components) toward very small residual anisotropies $r(\infty)$ at long times. This suggested that femtosecond energy transfers occur among bulk antenna Chls with essentially random Q_y orientations. However, excitation of far-red Chls (>700 nm) sometimes yields nonzero residual anisotropies (as expected, since the far-red Chls are few in number); the far-red anisotropies often exhibit more slowly decaying components. Savikhin et al. (1999) described an "anomalous" 710 → 680 nm anisotropy that initialized at $r(0) \sim -0.50$, decaying to a small residual anistropy with ~2.4 ps kinetics. The negative initial anisotropy arose because the perpendicular absorption difference signal was larger than the parallel signal ($\Delta A_\perp > \Delta A_\parallel$), suggesting the presence of a ~680 nm exciton level polarized perpendicular to a ~720 nm state of the same parentage (e.g., a dimeric Chl pair with upper and lower exciton levels near the respective wavelengths). In this work, we have studied anisotropies under 710 and 720 nm excitation, using probe wavelengths ranging from 675 to 720 nm; differences were examined between PS I complexes with open and closed reaction centers. The results are summarized in Fig. 7 and in Table 2.

The excitation wavelengths 710 and 720 nm produced very similar anisotropies. Because the spectrum of the frequency-doubled OPA pump pulses was typically ~13 nm fwhm, the OPA output wings were suppressed in some experiments using either a 710 nm interference filter (711 nm center wavelength, 5.2 nm bandwidth) or a 720 nm filter (720 nm, 5.5 nm bandwidth). This filtering had little effect on either the isotropic or anisotropic profiles. Hence, only the anisotropies excited at 720 nm (using the interference filter) are shown in Fig. 7. Although several of the corresponding isotropic profiles showed significant differences between open and closed reaction centers (previous section), no such differences were found in the anisotropies (aside from the fact that the residual anisotropies were not

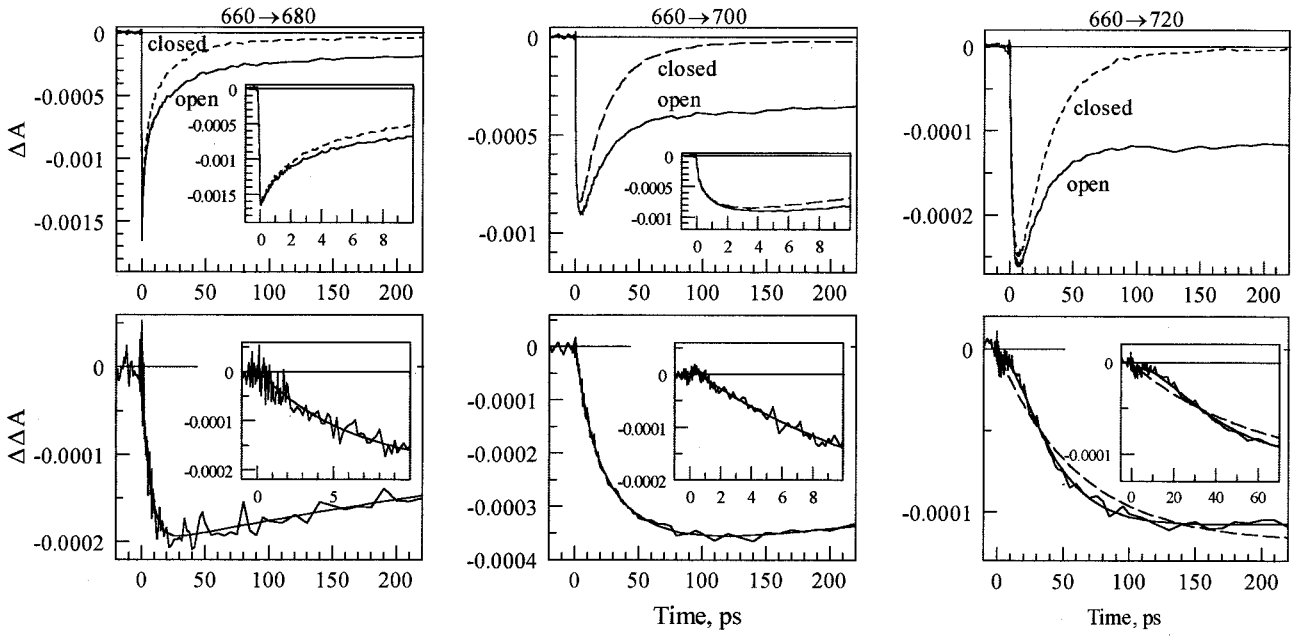

FIGURE 5 Isotropic absorption difference profiles for 660 → 680, 660 → 700, and 660 → 720 nm pump-probe experiments. Top row shows signals for open (*solid*) and closed (*dashed*) reaction centers; bottom row shows (open-closed) difference signal. Smooth curves show optimized fits to the difference signals (Table 1). *Insets* show signal on expanded time scales.

well defined due to low signals at long times). Hence, only the results for open reaction centers are shown in Fig. 7 and Table 2.

Single-exponential fits to the anisotropies yielded lifetimes ~10 ps; improved fits were obtained with biexponential models, with lifetimes of 1–2 ps and 11–20 ps (Table 2).

TABLE 1 Optimized parameters from local multiexponential fits to pump-probe profiles

pump → probe	τ_1 (a_1)	τ_2 (a_2)	τ_3 (a_3)	∞ (a_4)
660 → 680, open	0.40 (0.10)	2.2 (0.68)	23 (.66)	(0.26)
660 → 680, closed	0.40 (0.78)		21.0 (0.73)	(0.05)
660 → 680, open-closed	6.2 (−0.21)			(0.204)
660 → 690, open	0.37 (−0.44)	4.0 (0.39)	24.1 (1.34)	(−0.10)
660 → 690, closed	0.45 (−0.50)	3.9 (0.63)	21.1 (1.03)	(0.03)
660 → 690, open-closed	9.5 (−0.34)	25.3 (0.47)		(−0.13)
660 → 700, open	0.49 (−0.32)	2.2 (−0.47)	19.3 (0.69)	(0.42)
660 → 700, closed	0.33 (−0.24)	1.7 (−0.51)	21.9 (1.00)	(0.03)
660 → 700, open-closed	10.8 (−0.15)	37.6 (−0.26)		(0.04)
660 → 720, open	0.40 (0.05)	2.05 (−0.32)	22.1 (0.21)	(0.11)
660 → 720, closed	0.40 (0.04)	2.6 (−0.33)	27.0 (0.35)	(0.004)
660 → 720, open-closed	2.0 (−0.05)	6.0 (0.11)	30 (−0.17)	(0.11)
718 → 680, open		3.5 (−0.26)	44 (0.20)	(0.09)
718 → 680, closed		3.7 (−0.23)	27 (0.25)	(0.02)
718 → 680, open-closed		7.8 (−0.08)		(0.095)
718 → 690, open		2.5 (−0.23)	31 (0.60)	(−0.08)
718 → 690, closed		2.8 (−0.18)	27 (0.42)	(0.01)
718 → 690, open-closed		1.0 (−0.06)	47 (0.17)	(−0.09)
718 → 710, open		3.1 (0.25)	17 (0.27)	(0.18)
718 → 710, closed		3.1 (0.26)	23 (0.42)	(0.015)
718 → 710, open-closed			38 (−0.16)	(0.18)
718 → 720, open		3.2 (0.13)	17.5 (0.17)	(0.048)
718 → 720, closed		3.2 (0.12)	23 (0.22)	(0.003)
718 → 720, open-closed			68 (−0.054)	(0.054)

All lifetimes are in picoseconds.

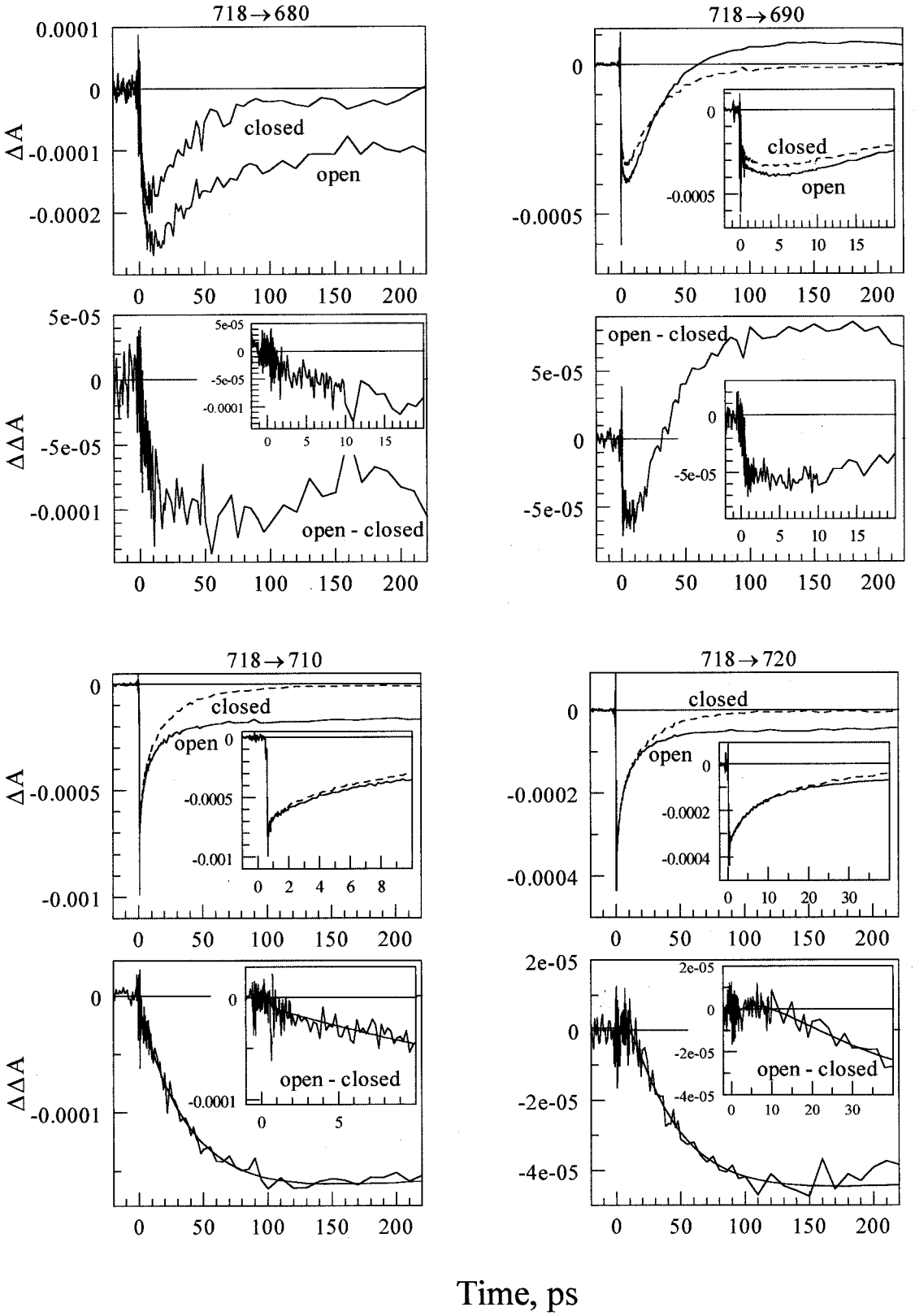

FIGURE 6 Isotropic absorption difference profiles obtained for PS I excited at 718 nm and probed at four different wavelengths: 680, 690, 710, and 720 nm. The top graph in each pair of panels shows signals for open and closed reaction centers, while the bottom graph shows the (open-closed) difference signal. Insets show expanded time scales.

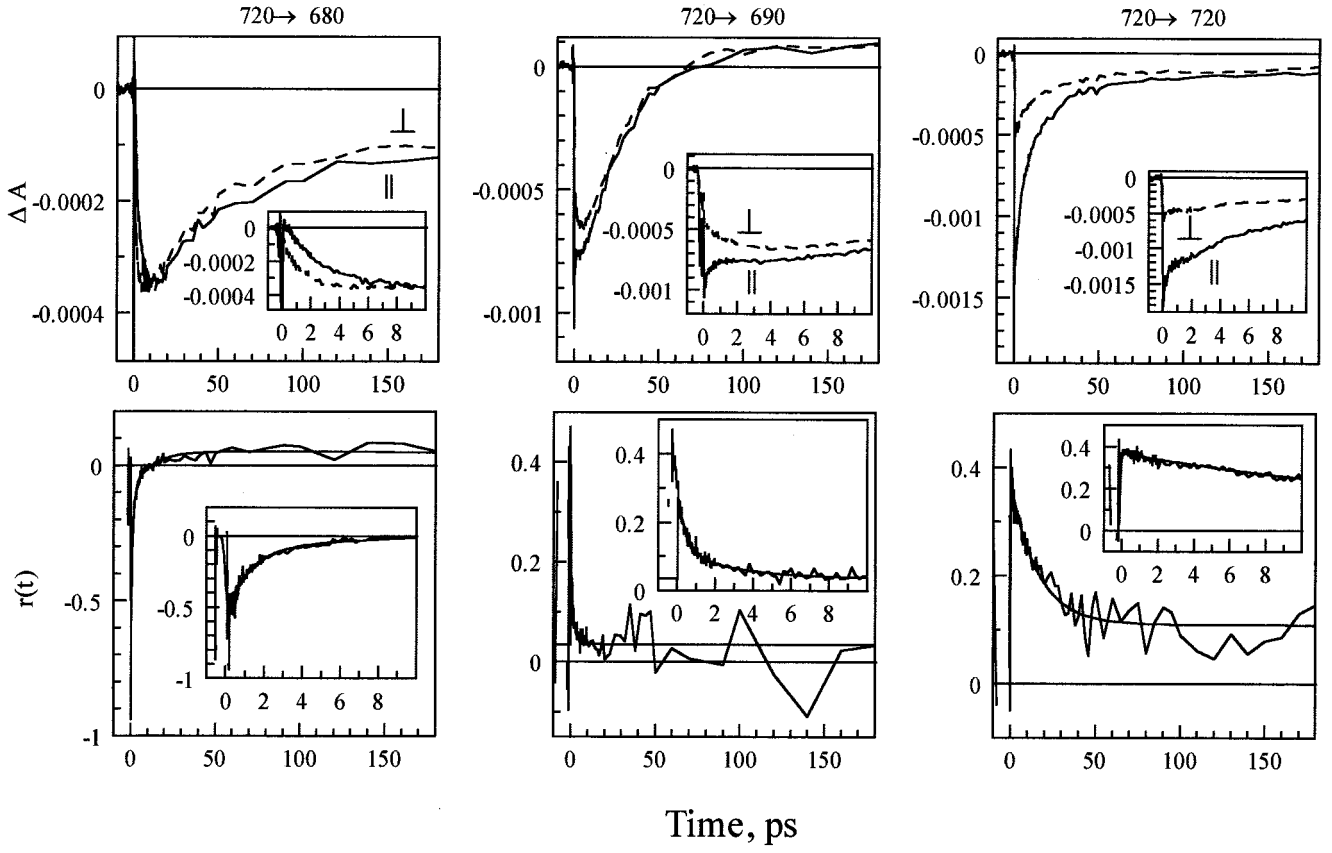

FIGURE 7 Polarized pump-probe profiles $\Delta A_{\parallel}(t)$, $\Delta A_{\perp}(t)$ and anisotropies $r(t)$ for PS I with open reaction centers, excited at 720 nm. Unlike isotropic signals (Fig. 6), the anisotropies show little dependence on the reaction center oxidation state.

An exception to this pattern was the anisotropy at 690 nm, whose decay was dominated by a 450 fs component followed by a slower 2–3 ps component. This was the only probe wavelength for which subpicosecond anisotropy decay was observed.

DISCUSSION

The steady-state (closed-open) PS I difference spectrum in Fig. 2 was analyzed by fitting with a sum of symmetric Gaussian components for wavelengths between 625 and 730 nm (Fig. 8). This spectrum is well described using a 10.5 nm fwhm Gaussian component centered at 691.3 nm (relative amplitude +6.5), combined with a 32.3 nm fwhm Gaussian at 698.2 nm (relative amplitude −5.0) and a 23.6 nm fwhm Gaussian at 655.6 nm (relative amplitude −1.6). The 698.2 nm band likely corresponds to the lower exciton component of the P700 special pair; its large fwhm is characteristic for charge-transfer transitions, which show large reorganization energies (Reddy et al., 1992; Pullerits et al., 1994; Rätsep et al., 2000). The sharper feature at 691.3 nm is assigned to the uncharged, monomeric Chl within the oxidized special pair ($P700^+$). Similar assignments were proposed for these two bands by Schaffernicht and Junge (1981). The relatively weak 655.6 "band" may not be a separate electronic transition, since it lies in the region of vibronic features of the main P700 and $P700^+$ Q_y bands at 698.2 and 691.3 nm. In this analysis, the relative areas under the P700 and $P700^+$ bands in the difference spectrum are 2.3:1. According to the 4 Å crystal structure of PS I from *Synechococcus elongatus*, the Q_y transition moments μ_A, μ_B of the special pair Chls are likely nearly parallel. For a P700 homodimer, the transition moments of the lower and upper transition moments would then be $\mu_{\pm} = (\mu_A \pm \mu_B)/\sqrt{2} \approx \sqrt{2}\mu_A$, 0. Hence, essentially all of the oscillator strength in the P700 exciton

TABLE 2 Optimized parameters from biexponential fits to anisotropies excited at 720 nm

	$r(t) = a_1 e^{-t/\tau_1} + a_2 e^{-t/\tau_2} + r(\infty)$		
pump → probe	τ_1 (a_1)	τ_2 (a_2)	$r(\infty)$
720 → 720	1.1 (0.04)	19 (0.24)	0.11
720 → 700	1.7 (0.06)	14 (0.18)	0.084
720 → 690	0.45 (0.15)	3.0 (0.08)	0.035
720 → 680	1.2 (−0.49)	13 (−0.14)	0.053

All lifetimes are in picoseconds.

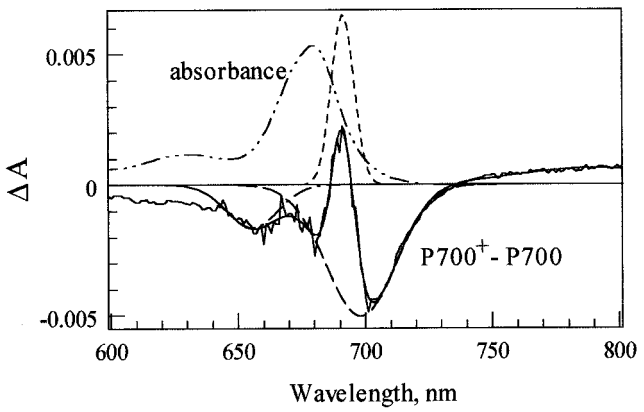

FIGURE 8 Decomposition of (open-closed) steady-state absorption difference spectrum for PS I complexes into sum of symmetric Gaussian components, with parameters given below. Individual spectral components are given by *long-dashed*, *short-dashed*, and *dot-dashed curves*; total simulated spectrum is given by smooth *solid curve* superimposed on experimental curve. The *dot-dot-dashed curve* shows steady state absorbance scaled by a factor of 0.01.

levels would be concentrated in the lower exciton level (at ~700 nm), which would then contain about twice the monomeric oscillator strength $\mu_A{}^2$. Schaffernicht and Junge (1981) proposed instead that the P700 band is a superimposition of the upper and lower exciton levels, i.e., that the exciton splitting is small compared to the bandwidth. More recent estimates for the P700 splitting are ~550 cm^{-1} (Vrieze et al., 1992) and ~370 cm^{-1} (Brettel, 1997). If P700 were homodimeric (and this is unknown), our analysis would suggest that the upper exciton level lies at ~680 nm, i.e., that the splitting is ~410 cm^{-1}. However, such a simple analysis does not consider the electrochromic effects of the charged Chl^+ on the spectrum of the neutral Chl in $P700^+$.

One of the key clues to early reaction center events in PS I appears to be the 660 → 690 nm experiment (Fig. 4), where the probe wavelength coincides with the absorption growth peak in the long-time ($P700^+$ - P700) difference spectrum (Fig. 3). The experimental kinetics of the (closed-open) absorption difference signal were fitted by

$$\Delta A(t) = 0.34\exp(-t/9.5\text{ ps}) - 0.47\exp(-t/25.3\text{ ps}) + 0.13\exp(-t/1100\text{ ps}) \quad (1)$$

where the amplitudes are in milliabsorption units. The longest-component lifetime is not well defined in the 200 ps time window of our experiment and is probably much longer than 1100 ps. The ratio of amplitudes for the 25.3 and 1100 ps components is 0.47/0.13 = 3.6. This is close to the ratio of amplitudes at 690 nm for the P700 (698.2 nm) and $P700^+$ (691.3 nm) Gaussian components in the $P700^+$ - P700 steady-state difference spectrum, 0.043/0.015 = 2.9. This suggests that the 660 → 690 nm (open-closed) difference profile in Fig. 4 *c* is largely a superimposition of PB/SE rise kinetics in the P700 spectrum centered at 700 nm (due to energy transfer from the antenna), combined with absorption rise kinetics in the $P700^+$ spectrum centered at 690 nm (due to creation of the 690 nm monomeric Chl species). The two processes would then exhibit contrasting kinetics, with the distinct lifetimes 9.5 and 25.3 ps. This, in turn, implies that P700+ formation does not occur simultaneously with P700 photobleaching. Contributions from the (A_0^- - A_0) difference spectrum should be considered a priori. However, it is unlikely to influence our observed kinetics in this interpretation, due to small A_0^- population buildup (see below).

We analyze our kinetics with the sequential kinetic scenario:

$$\text{antenna*P700 } A_0\text{ X} \xrightarrow{\tau_1} \text{antenna P700* } A_0\text{ X} \xrightarrow{\tau_2} \text{antenna P700}^+\ A_0^-\text{ X} \xrightarrow{\tau_3} \text{antenna P700 } A_0\text{ X}$$

Here antenna* denotes an antenna with electronic excitation, P700* denotes electronically excited P700 (or zwitterionic $^+P700^-$), and X collectively denotes the remainder of the electron transfer chain, A_1 - F_X - $F_{A/B}$. The lifetime for the last step, which includes charge recombination, recovering original ground state PS I with open reaction centers under dark conditions, is of course several orders of magnitude longer than the timescales considered here. Our experiments do not directly probe the kinetics of A_1 or the iron-sulfur centers, which do not absorb in the monitored spectral region. Solution of the kinetic equations for this scenario leads to the time-dependent populations

$$\begin{aligned} N_1(t) &= e^{-t/\tau_1} \\ N_2(t) &= \frac{\tau_2}{\tau_2-\tau_1}e^{-t/\tau_2} + \frac{(\tau_1-\tau_3)\tau_2}{\tau_1^2-\tau_1\tau_2-\tau_1\tau_3+\tau_2\tau_3}e^{-t/\tau_1} \\ N_3(t) &= \frac{\tau_3^2}{(\tau_1-\tau_3)(\tau_2-\tau_3)}e^{-t/\tau_3} - \frac{\tau_2\tau_3}{(\tau_1-\tau_2)(\tau_2-\tau_3)}e^{-t/\tau_2} \\ &\quad + \frac{\tau_1\tau_3}{\tau_1^2-\tau_1\tau_2-\tau_1\tau_3+\tau_2\tau_3}e^{-t/\tau_1} \end{aligned} \quad (2)$$

where $N_1(t)$ is the population for the state [antenna* P700 A_0 X], $N_2(t)$ is that for [antenna P700* A_0 X], and $N_3(t)$ is that for [antenna $P700^+$ A_0^- X]. If the antenna kinetics at this probe wavelength are not greatly affected by the P700 oxidation state, the components arising from $N_1(t)$ would cancel in the (open-closed) absorption difference profile. In our model, growth in the population N_2 causes photobleaching of the excitonic P700 spectrum, whereas growth in N_3 causes absorption rise behavior in the monomeric Chl spectrum centered at 690 nm (due to buildup of $P700^+$). For times *t* short compared to τ_3, and when $\tau_3 \gg (\tau_1, \tau_2)$, the

populations reduce into

$$N_1(t) = e^{-t/\tau_1}$$
$$N_2(t) = \frac{\tau_2}{\tau_2 - \tau_1} e^{-t/\tau_2} - \frac{\tau_2}{\tau_2 - \tau_1} e^{-t/\tau_1} \quad (3)$$
$$N_3(t) = 1 - \frac{\tau_2}{\tau_2 - \tau_1} e^{-t/\tau_2} + \frac{\tau_1}{\tau_2 - \tau_1} e^{-t/\tau_1}$$

It is important to recognize that $N_2(t)$ builds up with a rise time equal to the shorter of (τ_1, τ_2), and decays with lifetime equal to the longer of (τ_1, τ_2), regardless of the order in which these lifetimes appear in the mechanism. For example, for $\tau_1 = 20$ ps and $\tau_2 = 10$ ps, which are similar to the lifetimes 25.3 and 9.5 ps in Eq. 1,

$$N_2(t) = \exp(-t/20\text{ ps}) - \exp(-t/10\text{ ps})$$

If the same numerical lifetimes appear in reverse order in this mechanism (i.e., $\tau_1 = 10$ ps and $\tau_2 = 20$ ps), the population $N_2(t)$ becomes

$$N_2(t) = 2[\exp(-t/20\text{ ps}) - \exp(-t/10\text{ ps})]$$

i.e., it exhibits the same rise and decay times (the same shape), but with amplitude scaled by the factor $\tau_2/(\tau_1 + \tau_2)$. Furthermore, the population $N_3(t)$ is independent of the order in which τ_1 and τ_2 are assigned. The choice $\tau_1 =$ 20–25 ps is reasonable here, because it corresponds to the known antenna decay kinetics under annihilation-free conditions (Hastings et al., 1995; Savikhin et al., 1999; Fig. 3 in the present paper). The 660 → 690 nm (open-closed) difference kinetics were fitted using Eq. 3, yielding the optimized lifetimes $\tau_1 = 22.6$ ps and $\tau_2 = 10.2$ ps. The 22.6 ps component stems from antenna excitation trapping at P700. The 10.2 ps step (which may correspond to the "4 ps" kinetics observed by Hastings et al. (1994b) in their 590 → 686 nm (open-closed) difference profile under lower signal/noise ratio) would then reflect the kinetics of the P700* → A_0 electron transfer, [P700* A_0] → [$P700^+$ A_0^-]. We note here that the relative amplitudes of the components with lifetime τ_1 and τ_2 are fixed in the two-parameter model of Eq. 3; i.e., there is no leeway for independently adjusting the amplitudes to fit the 660 → 690 nm (open-closed) difference spectrum. The model predicts the experimental amplitude ratio in Fig. 4 for these components to within 20%, using the pertinent values of the Gaussian spectra for P700 and $P700^+$ at 690 nm (Fig. 8). This suggests that additional differential spectral changes (e.g., arising from A_0 reduction/oxidation or changes in antenna kinetics) are not major contributors to the observed kinetics in the 660 → 690 nm experiment. (It also supports the assignments of the lifetimes 22.6 ps and 10.2 ps to τ_1 and τ_2, respectively, instead of the reverse.) The 686 nm (A_0^- - A_0) difference spectrum reported by Hastings et al. (1994b) appears to be due in part to the developing $P700^+$ photobleaching spectrum (band maximum near 690 nm, cf. Fig. 8). This band persists at long times in experiments on PS I complexes with open reaction centers (Fig. 3). Hastings et al. concluded that the A_0 reduction and re-oxidation timescales are both on the order of 20 ps under annihilation-free conditions. Although our experiments suggest instead that the P700*A_0 →$P700^+A_0^-$ step occurs with 10.2 ps kinetics, they shed no light on the kinetics of the $A_0 \rightarrow A_1$ electron transfer. A very recent study by Brettel and Vos (1999), who monitored absorption changes at 390 nm, suggests that the overall upper limit to the timescale of A_1 reduction after antenna excitation is ~30 ps. (It should be cautioned that some of the absorption at this wavelength arises from antenna Chls, so that these experiments do not necessarily isolate the A_1 kinetics from antenna processes.) Because antenna excitation trapping at P700 requires some 20–25 ps, this would imply that the rate of A_0^- re-oxidation is comparable to or faster than the ~10 ps A_0^- formation rate. This would minimize its buildup and photobleaching signal. Finally, our 9–10 ps lifetime represents an upper limit to the P700 → A_0 electron transfer time, because the empirical $P700^+$ absorption kinetics may encompass relaxation processes (e.g., vibrational cooling) within $P700^+$ after the electron transfer step.

An alternative model, one which attributes the 690 nm kinetics to a combination of A_0 photobleaching and monomeric C690 absorption, can explain our data, but it would require independent assumptions. In this model, A_0 is quickly reduced ($\ll$ 10 ps) upon excitation trapping at P700. In the context of Eq. 3, the populations N_2 and N_3 would represent the states $P700^+$ A_0^- A_1 and $P700^+$ A_0 A_1^-, respectively. The 9–10 ps kinetics would be attributed to the overall electron transfer process P700 A_0 A_1 → $P700^+$ A_0 A_1^-, not to the individual P700 A_0 → $P700^+A_0^-$ step. The ~23 ps kinetics would still correspond to antenna excitation trapping at the reaction center. In this mechanism, growth in the population N_2 would cause a combination of PB rise in the broad P700 spectrum, PB rise in an A_0 spectrum centered at ~690 nm, and absorption rise due to monomeric C690. Subsequent decay of population N_2 into N_3 (during which A_0^- is reoxidized into A_0) would cause subsequent PB decay across the A_0 spectrum. The phenomenological "PB rise and decay times" observed at 690 nm would be ~9–10 and 20–25 ps, as is observed. Analysis of our absorption difference amplitudes using Eq. 3 shows that under this scheme, the absorption spectrum of unreduced A_0 would have to be nearly isobestic with that of the monomeric C690 species, with comparable absorption coefficient. In other words, the absorption differences caused by creation of P700* A_0 or $P700^+$ A_0^- would be nearly the same, so that PB of the A_0 spectrum would be cancelled by the absorption of monomeric C690 within $P700^+$. Subsequent electron transfer to A_1 would then cause PB decay in the A_0 spectrum, which would then no longer mask the monomeric C690 absorbance.

Close inspection of the 718→720 nm (open-closed) isotropic difference profile at early times (Fig. 6) indicates that

this signal consists of (i) a small, prompt PB/SE component which decays with ~6 ps kinetics (the error bounds for the latter lifetime are 3–9 ps due to noise) and (ii) a second, larger PB/SE component that initializes to zero and forms with 20–40 ps rise kinetics. The ratio of the respective PB/SE amplitudes is ~1:10, which is comparable to the fraction of light absorbed by P700 at this excitation wavelength (preceding paragraph). Hence, we attribute the smaller component to SE of directly excited P700, which transfers an electron to A_0 within ~9 ps. (This argues against the alternative model described above, in which the initial P700 $\rightarrow$ A_0 electron transfer occurs much faster than 10 ps.) The larger component arises at longer times as part of the red wing in the P700 PB/SE spectrum; its far larger amplitude derives from the fact that excitation placed in the more numerous Chls other than P700 at 718 nm ultimately results in bleaching of P700. We see no clear evidence of subpicosecond processes in any of the pump-probe experiments pumped at 718 nm, even though a non-negligible fraction of the light at this wavelength is directly absorbed by P700. This, coupled with the relatively slow development of the monomeric $P700^+$ absorption band near 690 nm, indicates that electronically excited P700* does not transfer an electron to A_0 with femtosecond kinetics. However, the initial charge separation itself (forming $^+P700^-$ from P700*) would not necessarily cause additional absorption changes in this spectral region, and this may well be an ultrafast trapping step.

The relative contribution of the P700 band to the total PS I steady-state absorption spectrum at far-red wavelengths has always been difficult to assess, owing to the small PS I absorption coefficients for $\lambda > 700$ nm. Order-of-magnitude estimates are afforded by our absorption difference profiles excited at 718 nm in open reaction centers (Fig. 6). The signal at long times is dominated at these wavelengths by PB/SE of the P700 band in the asymptotic ($P700^+$ - P700) absorption difference spectrum. The ratio of the instantaneous signal (which arises from PB/SE of all Chls absorbing at ~720 nm) to the long-time signal (due to residual P700 PB) in the 718 $\rightarrow$ 720 nm profile for open reaction centers is ~8:1, implying that P700 accounts for the order of ~1/10 of the total absorption near 720 nm at room temperature. The remainder of the steady-state absorption at that wavelength arises in part from the far-red Chls (the C714 and C708 Chls; Gobets et al., 1994; Rätsep et al., 2000), and in part from hot-band absorption by bulk antenna Chls absorbing at wavelengths <700 nm. By similar reasoning, P700 accounts for ~1/25 of the total absorption at 700 nm. (This is in accord with the statement by Hastings et al. (1994b) that selective excitation of P700 is not possible in physiological PS I complexes.) Direct comparison of the total steady state spectrum and the difference spectrum also indicates that the ratio of total to P700 absorbances at 710–720 nm is ~10 (Fig. 2.) Hence, some 90% of the light absorbed at 718 nm in room-temperature pump-probe experiments excites pigments other than the special pair Chls; the remainder is deposited in P700.

The 720 $\rightarrow$ 680 anisotropy decay (Fig. 7) is particularly interesting, because its negative initial value $r(0)$ suggests the presence of mutually orthogonally polarized exciton components near 720 and 680 nm, arising from strongly coupled Chls. This anisotropy, already reported by Savikhin et al. (1999), is identical in PS I with open and closed reaction centers. A broad 714 nm absorption feature identified in the 4.2 K spectral hole-burning of PS I core complexes from *Synechocystis* sp. (Rätsep et al., 2000) likely arises from a transition to the lower exciton component of strongly coupled, perhaps dimeric, Chls, which possesses significant charge transfer character. It was speculated in Savikhin et al. (1999) that the exciton components viewed in the 718 $\rightarrow$ 680 nm anisotropy may arise from the special pair Chls. However, the fact that the anisotropies are independent of reaction center oxidation state excludes this possibility. These anisotropies are therefore due not to P700, but to other excitonically coupled Chls in the PS I reaction center-core antenna complex. The absence of analogous anisotropies attributable to the P700 exciton components may be a consequence of low oscillator strength in the higher P700 exciton component.

SUMMARY

In a previously held scenario for the earliest reaction center events (Hastings et al., 1994b), excitation trapping from the antenna to the primary electron donor P700 occurs with 20–25 ps kinetics under annihilation-free conditions. The subsequent electron transfer step from P700 to A_0 is much faster than this, so the formation of the radical pair ($P700^+$ A_0^-) is essentially limited by the kinetics of excitation trapping from the antenna. Electron transfer to the secondary acceptor A_1 then occurs with ~20 ps kinetics, which nearly coincides with the antenna trapping kinetics within experimental error. This was not an unreasonable scenario, given the information available at the time.

We agree that antenna excitation trapping at P700 proceeds with 20–25 ps kinetics (cf. Fig. 3). However, we believe that formation of the radical pair upon trapping is not instantaneous on the experimental timescale. The process that forms the radical pair ($P700^+$ A_0^-) from the excited primary donor state (P700* A_0) itself requires some 9–10 ps. By comparison, the analogous electron transfer from the primary donor state to the bacteriopheophytin (which likely proceeds *via* an intermediate radical pair $p + B^-$; Zinth and Kaiser, 1993) is complete within ~3 ps in purple bacterial reaction centers. In photosystem II, the corresponding process is formation of the radical pair $P680^+Pheo^-$. As in PS I, the kinetics of this step are not easily separated from those of other primary processes, such as energy transfer to the reaction center core from surrounding pigments. The majority view of the charge separation rate in photosystem II is

typified by Roelofs et al. (1991, 1993) and Schelvis et al. (1994), who concluded that this occurs with 2–3 ps kinetics (as in purple bacterial reaction centers). However, experiments by Klug and coworkers (Durrant et al., 1992, 1993; Hastings et al., 1992) suggest that a major fraction of the Pheo electron acceptor is reduced with ~20 ps kinetics. In a time-resolved absorption study of photosystem II from spinach, the population rise kinetics of $P680^+Pheo^-$ were well described by a 2.4-ps global component (Müller et al., 1996). In a minimal kinetic model that explained many of their transient features, these authors assigned an effective rate constant of 120 ns^{-1} (i.e., $(8.3\ ps)^{-1}$) to the charge separation step. Since excitations in the photosystem II reaction center core were not believed to be localized on P680, it was concluded that the intrinsic charge separation rate constant was higher than this by a factor of ~3. This would bring the intrinsic charge separation rate for photosystem II in line with the time scale found in purple bacterial reaction centers.

The kinetics of the $A_0 \rightarrow A_1$ electron transfer, which are not reflected by our experiments because we see no evidence for an independent transient spectrum attributable to $(A_0^- - A_0)$, are still unknown. We do not believe that the 686 nm spectrum that has been previously ascribed to $(A_0^- - A_0)$ necessarily arises from that species; this phenomenon arises at least in part from evolution of the monomeric 690 nm Chl feature in the long-time ($P700^+ - P700$) spectrum.

The apparent antenna kinetics may depend somewhat on the P700 oxidation state. A major 6.5 ps component arises in global analysis of the PS I kinetics for closed reaction centers, and such a component does not appear for open reaction centers (Fig. 3). It is unclear whether this difference stems from antenna kinetic adjustments due to changes in the reaction center, or whether they arise from reaction center processes specific to open reaction centers. Simulations of the PS I antenna kinetics predict that oxidizing the reaction center will produce detectable changes in the antenna kinetics themselves (Savikhin and Struve, unpublished work). Nevertheless, the overall experimental trapping times are remarkably similar for PS I complexes with open and closed reaction centers (23.5 vs. 24 ps), in agreement with prior observations by several other groups.

Research at the Ames Laboratory was supported by Division of Chemical Sciences, Office of Basic Energy Sciences, U. S. Department of Energy. Ames Laboratory is operated by Iowa State University under Contract W-7405-Eng-82.

This research was supported by NSF grant MCB0078264 (to P.R.C.).

REFERENCES

Allen, J. P., G. Feher, T. O. Yeates, D. C. Rees, J. Deisenhofer, H. Michel, and R. Huber. 1986. Structural homology of reaction centers from *Rhodobacter sphaeroides* and *Rhodopseudomonas viridis* as determined by x-ray diffraction. *Proc. Natl. Acad. Sci. USA.* 83:8589–8593.

Brettel, K. 1997. Electron transfer and arrangement of the redox cofactors in photosystem I. *Biochim. Biophys. Acta.* 1318:322–373.

Brettel, K., and M. H. Vos. 1999. Spectroscopic resolution of the picosecond reduction kinetics of the secondary acceptor A_1 in photosystem I. *FEBS Lett.* 447:315–317.

Chang, C.-H., O. El-Kabbani, D. Tiede, J. Norris, and M. Schiffer. 1991. The structure of the membrane-bound protein photosynthetic reaction center from *Rhodobacter sphaeroides. Biochemistry.* 30:5352–5360.

Deisenhofer, J. O. Epp, R. Miki, R. Huber, and H. Michel. 1985. Structure of the protein subunits in the photosynthetic reaction centre of *Rhodopseudomonas viridis* at 3 Å resolution. *Nature.* 318:618–624.

Deisenhofer, J., and H. Michel. 1989. The photosynthetic reaction centre from the purple bacterium *Rhodopseudomonas viridis. EMBO J.* 8:2149–2169.

Du, M., X. Xie, Y. Jia, L. Mets, and G. R. Fleming. 201. 1993. Direct observation of ultrafast energy transfer in PS I core antenna. *Chem. Phys. Lett.* 201:535–542.

Durrant, J. R., G. Hastings, Q. Hong, J. Barber, G. Porter, and D. R. Klug. 1992. Determination of P680 singlet state lifetimes in photosystem two reaction centers. *Chem. Phys. Lett.* 188:54–60.

Durrant, J. R., G. Hastings, D. M. Joseph, J. Barber, G. Porter, and D. R. Klug. 1993. Rate of oxidation of P680 in isolated photosystem two reaction centers monitored by loss of chlorophyll stimulated emission. *Biochemistry.* 32:8259–8267.

Gobets, B., H. van Amerongen, R. Monshouwer, J. Kruip, M. Rögner, R. van Grondelle, and J. P. Dekker. 1994. Polarized site-selected fluorescence spectroscopy of isolated photosystem I particles. *Biochim. Biophys. Acta.* 1188:75–85.

Hasson, K. C. 1997. Time-resolved studies of the protein bacteriorhodopsin using femtosecond laser pulses. Ph.D. thesis, Harvard University, Cambridge, MA.

Hastings, G., J. R. Durrant, J. Barber, G. Porter, and D. R. Klug. 1992. Observation of pheophytin reduction in Photosystem Two reaction centers using femtosecond transient absorption spectroscopy. *Biochemistry.* 31:7638–7647.

Hastings, G., F. A. M. Kleinherenbrink, S. Lin, and R. E. Blankenship. 1994a. Time-resolved fluorescence and absorption spectroscopy of photosystem I. *Biochemistry.* 33:3185–3192.

Hastings, G., F. A. M. Kleinherenbrink, S. Lin, and R. E. Blankenship. 1994b. Observation of the reduction and reoxidation of the primary electron acceptor in photosystem I. *Biochemistry.* 33:3193–3.

Hastings, G., S. Hoshina, A. N. Webber, and R. E. Blankenship. 1995. Universality of energy and electron transfer processes in photosystem I. *Biochemistry.* 34:15512–15522.

Hecks, B., K. Wulf, J. Breton, W. Leibl, and H.-W. Trissl. 1994. Primary charge separation in photosystem I: a two-step electrogenic charge separation connected with $P700^+A0^-$ and $P700^+A_1^-$ formation. *Biochemistry.* 33:8619–8624.

Holzwarth, A. R., W. Haehnel, R. Ratajczak, E. Bittersmann, and G. H. Schatz. 1990. Energy transfer kinetics in photosystem I particles isolated from Synechococcus sp. and from higher plants. *In* Current Research in Photosynthesis. Baltscheffsky, M., editor. Kluwer Academic Publishers, Dordrecht. 611–614.

Holzwarth, A. R. 1991. Excited state kinetics in chlorophyll systems and its relationship to functional organization of the photosystems. *In* Chlorophylls. H. Scheer, editor. CRC Press, Boca Raton, FL. 1125–1151.

Holzwarth, A. R. 1992. Exciton dynamics in antennae and reaction centers of photosystems I and II. *In* Research in Photosynthesis. N. Murata, editor. Vol. I. Kluwer Academic Publishers, Dordrecht. 187–194.

Holzwarth, A. R., G. H. Schatz, H. Brock, and E. Bittersmann. 1993. Energy transfer and charge separation kinetics in photosystem I: 1. Picosecond transient absorption and fluorescence study of cyanobacterial photosystem I particles. *Biophys. J.* 64:1813–1826.

Ikegami, I., and S. Itoh. 1986. Chlorophyll organization in P-700-enriched particles isolated from spinach chloroplasts: CD and absorption spectroscopy. *Biochim. Biophys. Acta.* 851:75–85.

Jia, Y., J. M. Jean, M. M. Werst, C.-K. Chan, and G. R. Fleming. 1992. Simulations of the temperature dependence of energy transfer in the PS I core antenna. *Biophys. J.* 63:259–273.

Karapetyan, N. V., D. Dorra, G. Schweitzer, I. N. Bezsmertnaya, and A. R. Holzwarth. 1997. Fluorescence spectroscopy of the longwave chlorophylls in trimeric and monomeric photosystem I core complexes from the cyanobacterium *Spirulina platensis*. *Biochemistry.* 36:13830–13837.

Krauss, N., W. Hinrichs, I. Witt, P. Fromme, W. Pritzkow, Z. Dauter, C. Betzel, K. S. Wilson, H. T. Witt, and W. Saenger. 1993. Three-dimensional structure of system I of photosynthesis at 6 Å resolution. *Nature.* 361:326–330.

Krauss, N., W.-D. Schubert, O. Klukas, P. Fromme, H. T. Witt, and W. Saenger. 1996. Photosystem I. at 4 Å. resolution: a joint photosynthetic reaction center and core antenna system. *Nat. Struct. Biol.* 3:965–973.

Müller, M. G., M. Hucke, M. Reus, and A. R. Holzwarth. 1996. Primary processes and structure of the Photosystem II reaction center. 4. Low-intensity femtosecond transient absorption spectra of D1–D2-cyt-b559 reaction centers. *J. Phys. Chem.* 100:9527–9536.

Owens, T. G., S. P. Webb, L. Mets, R. S. Alberte, and G. R. Fleming. 1988. Antenna structure and excitation dynamics in photosystem I. I. Studies of detergent-isolated photosystem I preparations using time-resolved fluorescence analysis. *Biophys. J.* 53:733–745.

Pullerits, T., F. van Mourik, R. Monshouwer, R. W. Visschers, and R. van Grondelle. 1994. Electron phonon coupling in the B820 subunit form of LH1 studied by temperature dependence of optical spectra. *J. Luminescence* 58:168–171.

Rätsep, M., T. W. Johnson, P. R. Chitnis, and G. J. Small. 2000. The red-absorbing Chlorophyll *a* antenna states of photosystem I: A hole-burning study of *Synechocystis* PCC 6803 and its mutants. *J. Phys. Chem. B*104:836–847.

Reddy, N. R. S., P. A. Lyle, and G. J. Small. 1992. Applications of spectral hole burning spectroscopies to antenna and reaction center complexes. *Photosynth. Res.* 31:167–194.

Roelofs, T. A., M. Gilbert, V. A. Shuvalov, and A. R. Holzwarth. 1991. Picosecond fluorescence kinetics of the D_1-D_2-Cyt b-559 Photosystem II reaction center complex. Energy transfer and charge separation processes. *Biochim. Biophys. Acta.* 1060:237–244.

Roelofs, T. A., S. L. S. Kwa, R. van Grondelle, J. P. Dekker, and A. R. Holzwarth. 1993. Primary processes and structure of the Photosystem II reaction center. II. Low-temperature picosecond fluorescence kinetics of a D_1-D_2-Cyt b-559 reaction center complex isolated by short Triton exposure. *Biochim. Biophys. Acta.* 1143:147–157.

Savikhin, S., W. Xu, V. Soukoulis, P. R. Chitnis, and W. S. Struve. 1999. Ultrafast primary processes in photosystem I of the cyanobacterium *Synechocystis* sp. *PCC* 6803. *Biophys. J.* 76:3278–3288.

Schaffernicht, H., and W. Junge. 1981. Analysis of the complex band spectrum of P700 based on photoselection studies with photosystem I particles. *Photochem. Photobiol.* 34:223–232.

Schelvis, J. P. M., P. I. van Noort, T. J. Aartsma, and H. J. van Gorkom. 1994. Energy transfer, charge separation, and pigment arrangement in the reaction center of Photosystem II. *Biochim. Biophys. Acta.* 1184: 242–250.

Soukoulis, V., S. Savikhin, W. Xu, P. R. Chitnis, and W. S. Struve. 1999. Electronic spectra of PS I mutants: the peripheral subunits do no bind red chlorophylls in *Synechocystis* sp. *PCC* 6803. *Biophys. J.* 76:2711–2715.

Sun, J., K. An, P. Jin, V. P. Chitnis, and P. R. Chitnis. 1998. Isolation and characterization of photosystem I subunits from the cyanobacterium *Synechocystis* sp. *PCC* 6803. *Meth. Enzymol.* 297:124–139.

Trinkunas, G., and A. R. Holzwarth. 1994. Kinetic modeling of exciton migration in photosynthetic systems. 2. Simulations of excitation dynamics in two-dimensional photosystem I core antenna/reaction center complexes. *Biophys. J.* 66:415–429.

Turconi, S., G. Schweitzer, and A. R. Holzwarth. 1993. Temperature dependence of picosecond fluorescence kinetics of a cyanobacterial photosystem I particle. *Photochem. Photobiol.* 57:113–119.

van der Lee, J., D. Bald, S. L. S. Kwa, R. van Grondelle, M. Rögner, and J. P. Dekker. 1993. Steady-state polarized light spectroscopy of isolated photosystem I complexes. *Photosynth. Res.* 35:311–321.

van Grondelle, R., J. P. Dekker, T. Gillbro, and V. Sundström. 1994. Energy transfer and trapping in photosynthesis. *Biochim. Biophys. Acta.* 1187:1–65.

Vrieze, J., P. Gast, and A. J. Hoff. 1992. The structure of the photosystem I reaction center investigated with linear dichroic absorbance-detected magnetic resonance at 1.2 K. *In* Research in Photosynthesis. N. Murata, editor. Kluwer Academic Publishers, Dordrecht. 553–556.

Werst, M., Y. Jia, L. Mets, and G. R. Fleming. 1992. Energy transfer and trapping in photosystem I core antenna: a temperature study. *Biophys. J.* 61:868–878.

Zinth, W., and W. Kaiser. 1993. Time-resolved spectroscopy of the primary electron transfer in reaction centers of *Rhodobacter sphaeroides* and *Rhodopseudomonas viridis*. *In* The Photosynthetic Reaction Center, Vol. II. J. Deisenhofer and J. Norris, editors. Academic Press, London. 71–88.